PROCEEDINGS OF SCIENCE

The fractional analysis of mass composition measured by the Telescope Array FADC fluorescence detectors in hybrid mode

Jihyun Kim[a,*] **and Douglas Bergman**[a] **on behalf of the Telescope Array Collaboration**

[a] *Dept. of Physics & Astronomy and High Energy Astrophysics Inst., University of Utah, Utah, USA*

E-mail: jihyun@cosmic.utah.edu, bergman@physics.utah.edu

We have simulated the Telescope Array FADC fluorescence detecter and surface detector array dataset from Jan. 2008 through Nov. 2018 with CORSIKA generated MC sets using three high-energy interaction models: QGSJetII-04, EPOS-LHC, and Sibyll 2.3d, and with four separate nuclear species for each model: hydrogen, helium, nitrogen and iron. The simulation includes detector response characteristics both of the surface detector, done using GEANT4, and for the fluorescence detectors, using ray-tracing, atmospheric attenuation and trigger simulation. Using the model and species data in energy bins, we created template $X_{\max}$ distributions, and used these templates to find the fractions of each species that best match the hybrid data for each model. The fractional fit was performed using a Markov Chain MC method which allows sampling of the likelihood space of the fractions. We present the fractions for each model and show the correlations between the fit fractions.

7th International Symposium on Ultra High Energy Cosmic Rays (UHECR2024)
17-21 November 2024
Malargüe, Mendoza, Argentina

*Speaker

 ISSN 1824-8039 . Published by SISSA Medialab.

PoS(UHECR2024)098

1. Motivation

Telescope Array (TA) and Pierre Auger Observatory (Auger), through their Joint Composition Working Group, are working to understand the composition of ultra-high energy cosmic rays (UHECRs). To compare results accounting for systematics, TA has been simulating Auger observations. This involves representing $X_{\max}$ distributions with fractions of different nuclear species (protons, helium, nitrogen, and iron) and using these in full detector simulations. This work presents the fitting TA's $X_{\max}$ distributions in order to determine similar fractions.

2. Data

We use TA hybrid data from the Black Rock Mesa (BR) and Long Ridge (LR) fluorescence detectors taken through Nov. 2018 (10 years) [1]. This data has been used in previous TA compositions analyses and in TA & Auger working group comparisons [2]. The energy range is $10^{18.2}$–$10^{19.4}$ eV. The template $X_{\max}$ distributions of single-species data as accepted and analyzed by TA, have been generated in the same way as in the works cited above, but using three different high-energy interaction models: QGSJetII-04, Sibyll 2.3d, and EPOS-LHC.

3. Fitting

To determine the UHECR composition, we used a Markov Chain Monte Carlo (MCMC) to fit the observed $X_{\max}$ distributions with fractions of different nuclear species. Initially, we considered four species (protons, helium, nitrogen, and iron), but due to strong anti-correlation between helium and nitrogen, leading to unstable results, we reduced the model to three species (protons, nitrogen, and iron) for a more reliable fit.

We used the `emcee` [3] implementation of an MCMC, with a likelihood calculated from the Poisson probability to observe n_i data events in an $X_{\max}$ bin with the expectation μ_i from the vector of fractions $\mathbf{f}$ of the templates.

$$\mathcal{L}(\mathbf{f}) = \prod_i \frac{\mu_i(\mathbf{f})^{n_i} e^{\mu_i(\mathbf{f})}}{n_i!}$$

The MCMC fit results are shown in corner plots for the Sibyll 2.3d model in Figures 1–3. The other models have similar corner plots. Red lines indicate the fraction value for the maximum likelihood fraction fit, while blue lines indicate the range of fraction values within 1σ of the maximum. All three fractions are shown, although there are only two independent fractions. The upper-right corner contains the $X_{\max}$ distribution of the data compared to the best-fit result from the MCMC sampling.

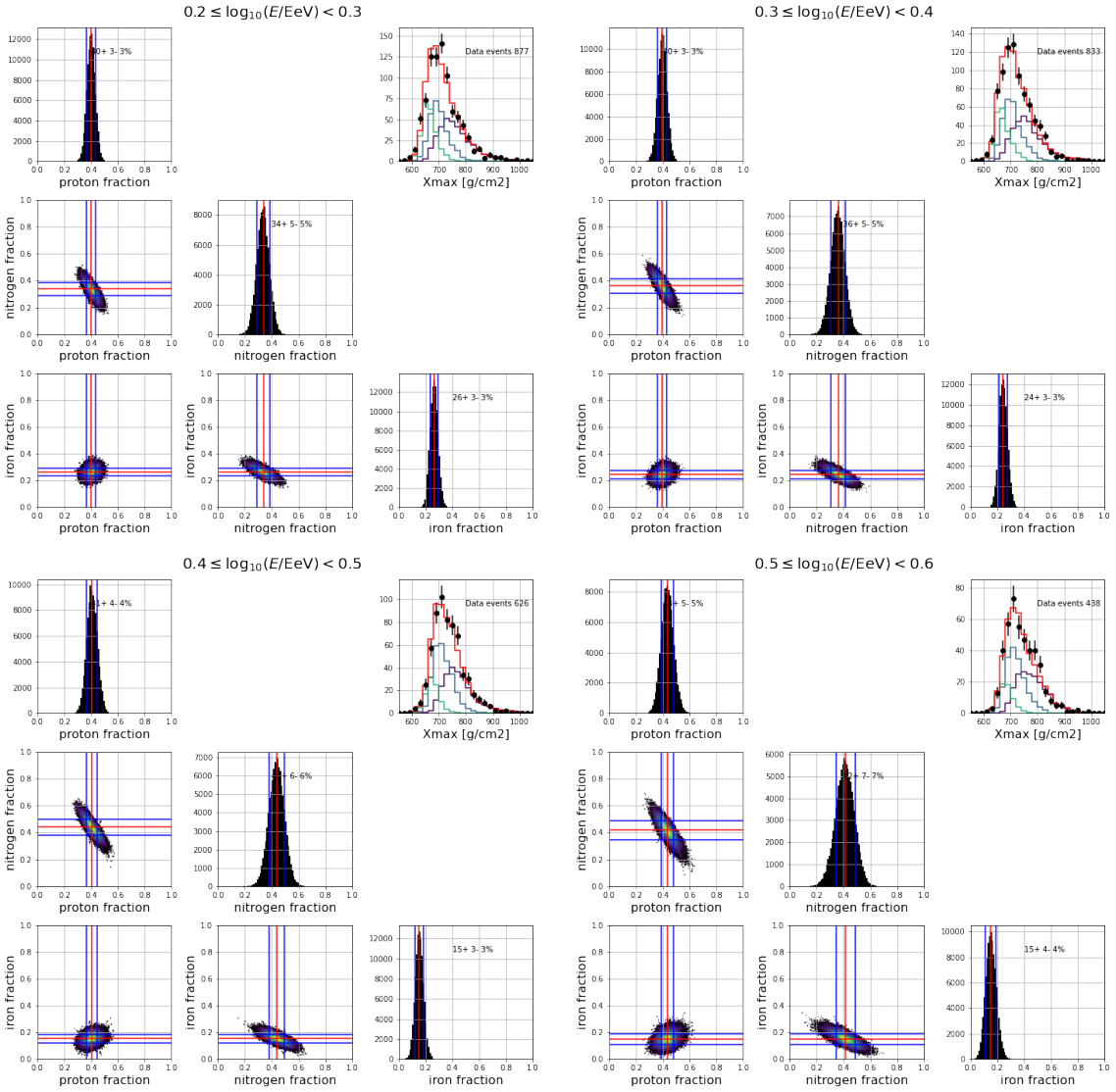

Figure 1: Corner plots of MCMC fraction fits to Sibyll 2.3d templates for data in energy bins $\log_{10} E/\mathrm{EeV}$ 0.2–0.3, 0.3–0.4, 0.4–0.5, and 0.5–0.6. The resulting match of the templates fit to the data is shown in the upper right corner. Histograms of the number of samples for each fraction value shown on the diagonal. Scatter plot of samples two fractions at a time shown in the lower triangle.

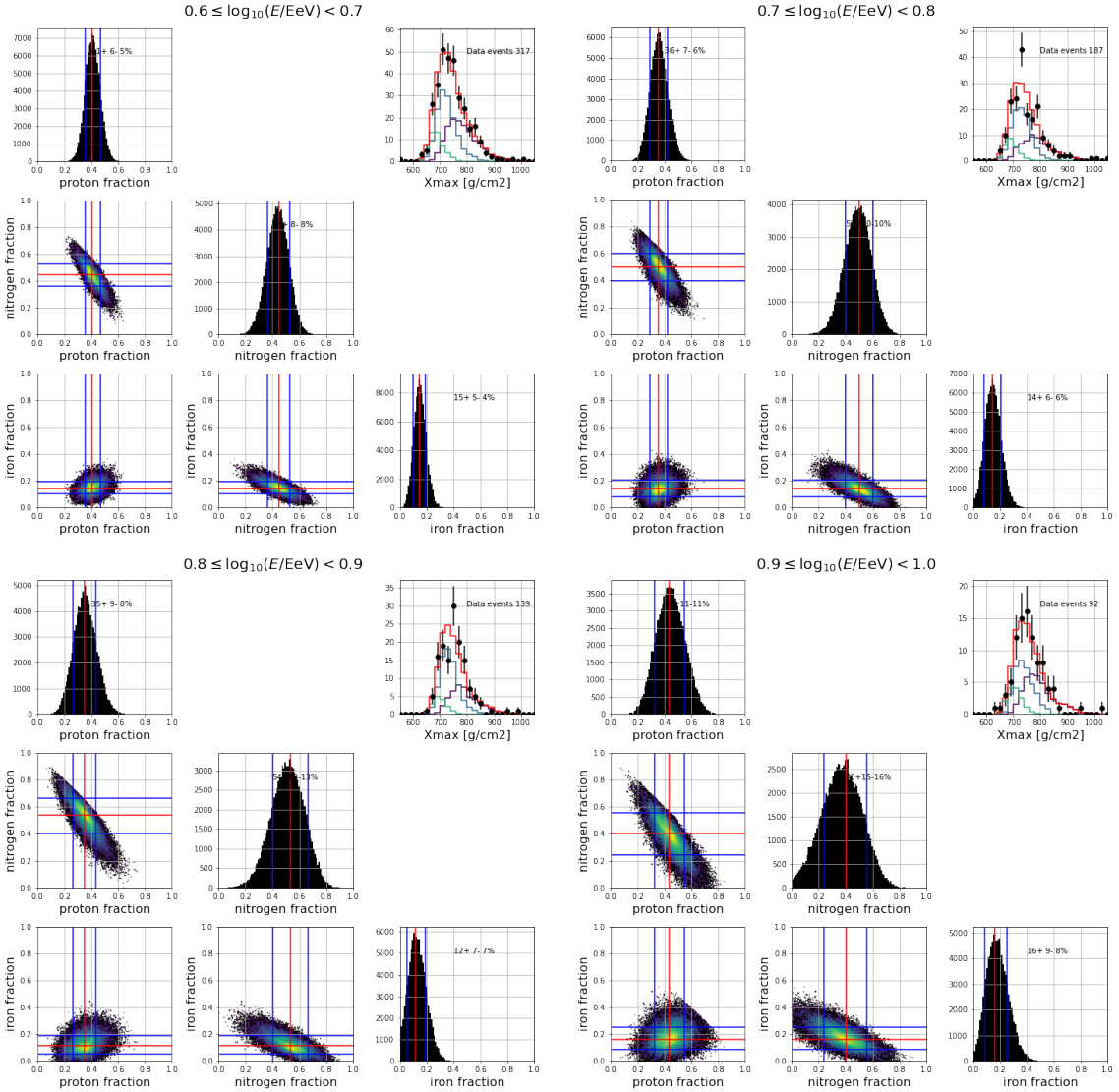

Figure 2: Corner plots of MCMC fraction fits to Sibyll 2.3d templates for data in energy bins $\log_{10} E/\mathrm{EeV}$ 0.6–0.7, 0.7–0.8, 0.8–0.9, and 0.9–1.0. Description of plots the same as in Figure 1.

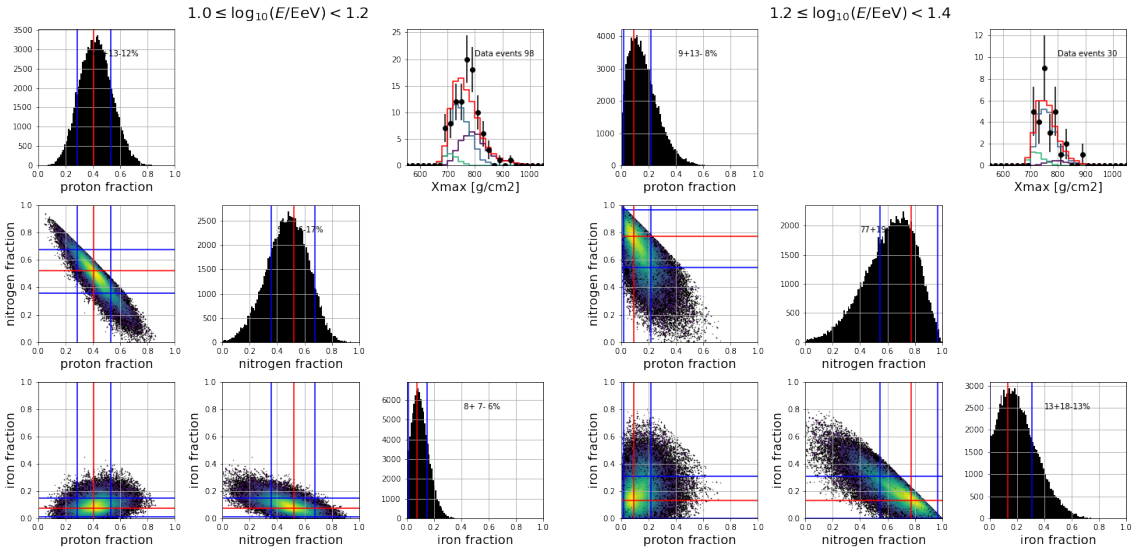

Figure 3: Corner plots of MCMC fraction fits to Sibyll 2.3d templates for data in energy bins $\log_{10} E/\mathrm{EeV}$ 1.0–1.2 and 1.2–1.4. Description of plots the same as in Figure 1.

4. Fractional Fit Results

The best-fit fractions from MCMC with 1σ uncertainties are given in Table 1 as percentages. The fractions are plotted, in the Figures 4 and 5. In the stacked plots, proton fraction uncertainties are shown the bottom, iron fraction uncertainties on top.

The fit should reproduce the mean and RMS of the data Comparisons are shown below the stacked histograms. We don't display the RMS with less than 50 events, which precludes a comparison of the width in the $1.2 \leq \log_{10}(E/\mathrm{EeV}) < 1.4$ bin. We also don't show any fit results for energies above $1.4 \leq \log_{10}(E/\mathrm{EeV})$ due to data statistics.

	QGSJetII-04			Sibyll 2.3d			EPOS-LHC		
$\log_{10}(E/\mathrm{EeV})$	proton	nitrogen	iron	proton	nitrogen	iron	proton	nitrogen	iron
0.2–0.3	56^{+4}_{-4}	33^{+7}_{-7}	11^{+4}_{-3}	40^{+3}_{-3}	34^{+5}_{-5}	26^{+3}_{-3}	50^{+4}_{-3}	21^{+5}_{-5}	29^{+3}_{-3}
0.3–0.4	52^{+4}_{-4}	45^{+6}_{-6}	3^{+4}_{-3}	40^{+4}_{-3}	36^{+5}_{-5}	24^{+3}_{-3}	55^{+3}_{-3}	16^{+5}_{-5}	29^{+3}_{-3}
0.4–0.5	68^{+5}_{-5}	30^{+6}_{-7}	2^{+3}_{-2}	41^{+4}_{-4}	44^{+6}_{-6}	15^{+3}_{-3}	58^{+4}_{-4}	27^{+5}_{-5}	15^{+3}_{-3}
0.5–0.6	69^{+4}_{-4}	31^{+5}_{-5}	0^{+2}_{-0}	43^{+5}_{-5}	42^{+4}_{-7}	15^{+4}_{-4}	58^{+4}_{-4}	23^{+6}_{-6}	20^{+4}_{-3}
0.6–0.7	70^{+6}_{-5}	26^{+7}_{-7}	4^{+4}_{-3}	41^{+6}_{-6}	45^{+8}_{-8}	15^{+5}_{-4}	52^{+5}_{-5}	29^{+7}_{-7}	19^{+5}_{-4}
0.7–0.8	57^{+8}_{-7}	43^{+7}_{-13}	0^{+7}_{-0}	36^{+7}_{-7}	50^{+10}_{-10}	14^{+6}_{-6}	49^{+7}_{-7}	31^{+10}_{-10}	20^{+6}_{-6}
0.8–0.9	62^{+8}_{-8}	38^{+8}_{-9}	0^{+3}_{-0}	35^{+9}_{-9}	54^{+13}_{-13}	12^{+7}_{-7}	46^{+8}_{-8}	38^{+12}_{-12}	15^{+7}_{-6}
0.9–1.0	63^{+11}_{-10}	37^{+11}_{-17}	1^{+9}_{-1}	44^{+11}_{-11}	40^{+15}_{-16}	16^{+9}_{-8}	57^{+11}_{-11}	26^{+14}_{-15}	18^{+8}_{-7}
1.0–1.2	83^{+12}_{-10}	17^{+10}_{-17}	0^{+6}_{-0}	40^{+13}_{-12}	52^{+16}_{-17}	8^{+7}_{-6}	67^{+10}_{-10}	16^{+14}_{-14}	17^{+7}_{-7}
1.2–1.4	37^{+18}_{-16}	63^{+16}_{-18}	0^{+5}_{-0}	9^{+13}_{-8}	78^{+19}_{-23}	13^{+18}_{-13}	20^{+15}_{-12}	56^{+19}_{-21}	25^{+14}_{-12}

Table 1: Fractional Fit Results

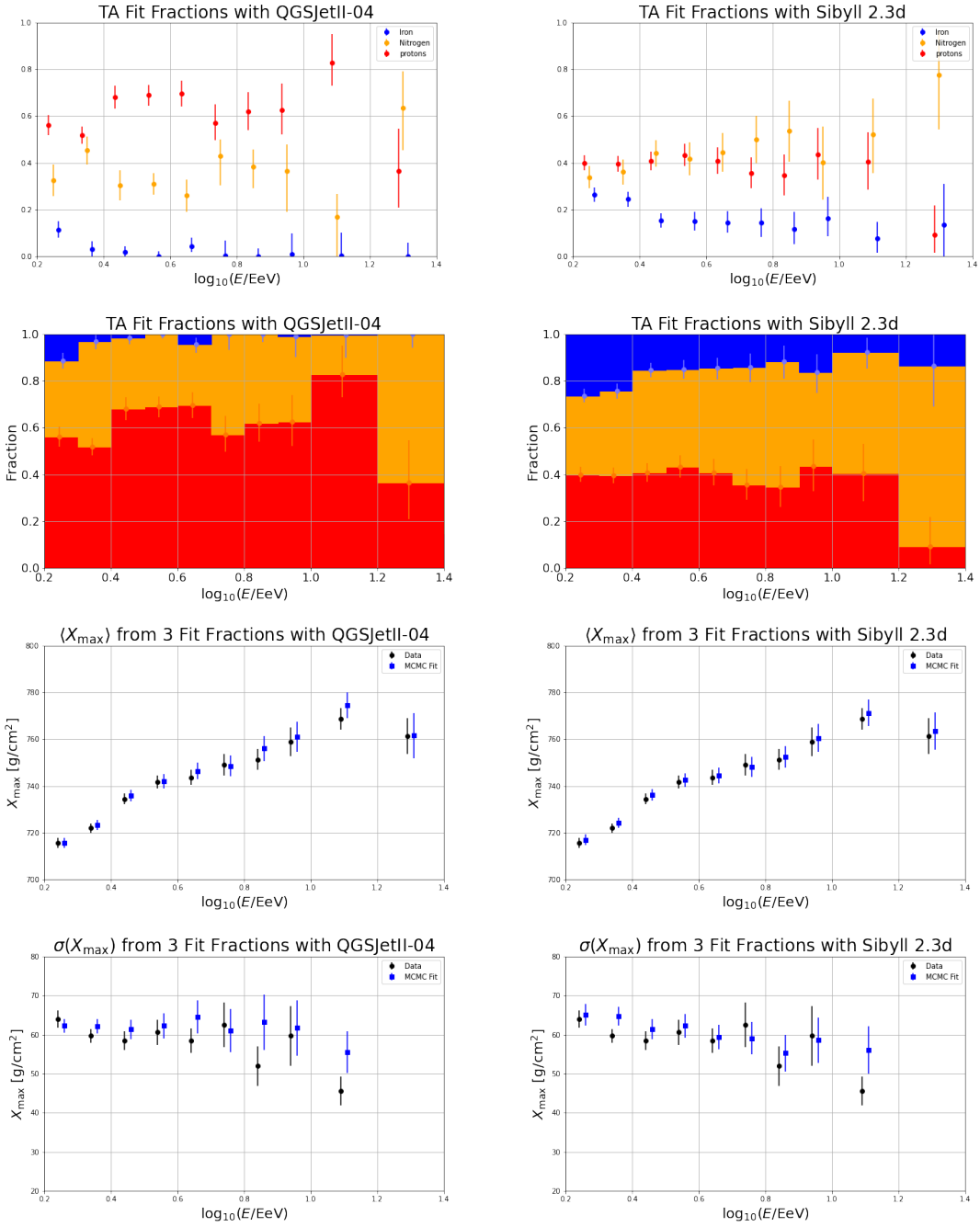

Figure 4: Result of fraction fits for QGSJetII-04 (left) and Sibyll 2.3d (right). Actual fractions (with errors) on first row, stacked fractions with H and Fe errors (inverted) second row, $\langle X_{\max} \rangle$ comparison of fit and data third row, $\sigma(X_{\max})$ comparison of fit and data fourth row.

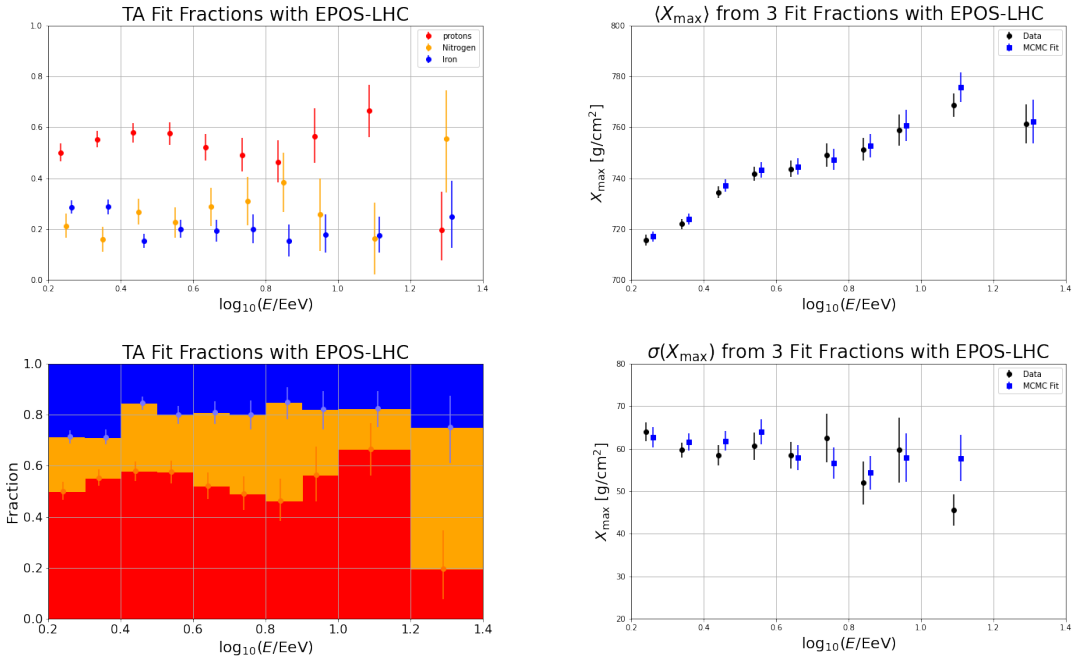

Figure 5: Result of fraction fits for EPOS-LHC. Actual fractions (with errors) upper left, stacked fractions with H and Fe errors (inverted) lower left, $\langle X_{\max} \rangle$ comparison of fit and data upper right, $\sigma(X_{\max})$ comparison of fit and data lower right.

References

[1] R.U. Abbasi *et al.*, Astrophys. J **858** (2018) 76.

[2] A. Yushkov, PoS(ICRC2023)249.

[3] D. Foreman-Mackey *et al.*, Pub. Ast. Soc. Pac. **125**. (2013) 306.

PoS(UHECR2024)098